

# Nanophotonic optical gyroscope with reciprocal sensitivity enhancement

Parham P. Khial <sup>\*</sup>, Alexander D. White  and Ali Hajimiri 

**Optical gyroscopes measure the rate of rotation by exploiting a relativistic phenomenon known as the Sagnac effect<sup>1,2</sup>. Such gyroscopes are great candidates for miniaturization onto nanophotonic platforms<sup>3,4</sup>. However, the signal-to-noise ratio of optical gyroscopes is generally limited by thermal fluctuations, component drift and fabrication mismatch. Due to the comparatively weaker signal strength at the microscale, integrated nanophotonic optical gyroscopes have not been realized so far. Here, we demonstrate an all-integrated nanophotonic optical gyroscope by exploiting the reciprocity of passive optical networks to significantly reduce thermal fluctuations and mismatch. The proof-of-concept device is capable of detecting phase shifts 30 times smaller than state-of-the-art miniature fibre-optic gyroscopes, despite being 500 times smaller in size. Thus, our approach is capable of enhancing the performance of optical gyroscopes by one to two orders of magnitude.**

Silicon nanophotonics is an ideal platform for implementing optical gyroscopes on the microscale due to its reliability and compatibility with current mass production techniques (Fig. 1a)<sup>5,6</sup>. Moreover, it can enable the integration of nanophotonic and electrical components onto a single substrate<sup>7–10</sup>.

Optical gyroscopes determine angular velocity by measuring the relativistic Sagnac effect<sup>11–13</sup>. When a beam of coherent light is split into two paths that traverse a closed circle (Fig. 1b), they meet with a certain phase relationship at the output. However, when the reference frame of the gyroscope is rotating, the effective path lengths experienced by the two beams change. This causes them to experience an additional time delay with respect to one another that is proportional to the rate of rotation of the frame<sup>12</sup>:

$$\Delta\varphi_{\text{Sagnac}} = \frac{8\pi n}{\lambda c} m\mathbf{A} \cdot \boldsymbol{\Omega} \quad (1)$$

where  $m\mathbf{A}$  is the area vector with magnitude equal to the area of the closed path multiplied by  $m$  (the number of turns),  $\boldsymbol{\Omega}$  is the angular velocity vector,  $n$  is the refractive index of the medium,  $\lambda$  is the wavelength, and  $c$  is the speed of light.

To measure the rates of rotation using the Sagnac effect, the input light beam in a typical optical gyroscope is split into two paths: the signal path, which is often coiled to accumulate the Sagnac phase shift, and the reference path. These two paths combine inside a phase interferometer whose output is proportional to the phase difference between the input signals<sup>14</sup>. As the system size is reduced (for example, in a nanophotonic optical gyroscope, NOG), the performance of this topology suffers from the small magnitude of the phase shift, which implies a low signal-to-noise ratio (SNR). This is because the Sagnac effect is proportional to the area enclosed by the optical path. This low SNR translates to

a stronger random walk in the output signal of the gyro, resulting in a poor Allan variance, a standard measure for characterizing the stability of gyroscopes<sup>15</sup>. Among all imperfections, the inevitable thermal drift is more pronounced because of the relatively large thermo-optic coefficient of silicon at room temperature:  $dn/dT = 1.86 \times 10^{-4} \text{K}^{-1}$ , where  $n$  is the index of silicon and  $T$  is the temperature in kelvin. Thus, even small temperature variations within different parts of the optical path can cause a considerable deviation in the measured rate of rotation. However, these temperature fluctuations in silicon nanophotonics have a bandwidth of several kilohertz<sup>16</sup>, are much less pronounced above a megahertz, and thus can be treated as constant over timescales of microseconds. In light of this observation, it is possible to significantly lower thermal fluctuations and other imperfections such as fabrication mismatch by intentionally alternating the polarity of the Sagnac phase shift at a fast rate, as shown conceptually in Fig. 1c.

To improve sensitivity we developed an approach we call reciprocal sensitivity enhancement. In a passive network made of isotropic elements (lossy or lossless), switching the input and output ports does not change the observed response from input to output. This is because the scattering matrix is symmetric, namely,  $S_{ij} = S_{ji}$  (note that  $S_{ij}$  is a complex number representing the phase and amplitude of the outgoing wave). By alternating the paths (the blue and red paths, as shown in Fig. 1c), two measurements are taken—one of  $S_{ij}$  and the other of  $S_{ji}$ —whereby the desired signal has its polarity flipped but undesirable components such as thermally induced fluctuations and mismatch are common and can therefore be attenuated.

Reciprocal sensitivity enhancement also reduces the undesirable effects of reflections. Although we know that reciprocal networks satisfy  $S_{ij} = S_{ji}$  for all  $i$  and  $j$ , in general  $S_{ii} \neq S_{jj}$  for  $i \neq j$ . This causes mismatch between reflected light from different directions, which poses a challenge for using continuous laser sources in existing architectures of single-loop gyroscopes that utilize both clockwise and anticlockwise beams<sup>12,17</sup>.

In a typical interferometry-based gyroscope architecture, light is sent in both clockwise and anticlockwise directions, and the phase shift induced by the Sagnac effect is measured at the output<sup>17–19</sup>. The sensitivity of these types of gyroscope is limited by the Kerr effect, unequal thermal fluctuations between clockwise and anticlockwise propagating light, and Rayleigh scattering<sup>20</sup>. The latter two are usually dominant. However, it has been demonstrated that the effect of back-scattering light can be reduced by using a non-coherent laser source<sup>17</sup>. Another approach to alleviate the issue of scattering is to use a low-loss waveguide, which usually demands a different waveguide core and clad material. In addition, some methods have been proposed to enhance the Sagnac effect and to boost the overall SNR<sup>21–23</sup>. Time-division switching can be used to reduce the back-scattering effect in fibre-optic gyroscopes<sup>24</sup>. Among all these methods, however, reciprocal sensitivity

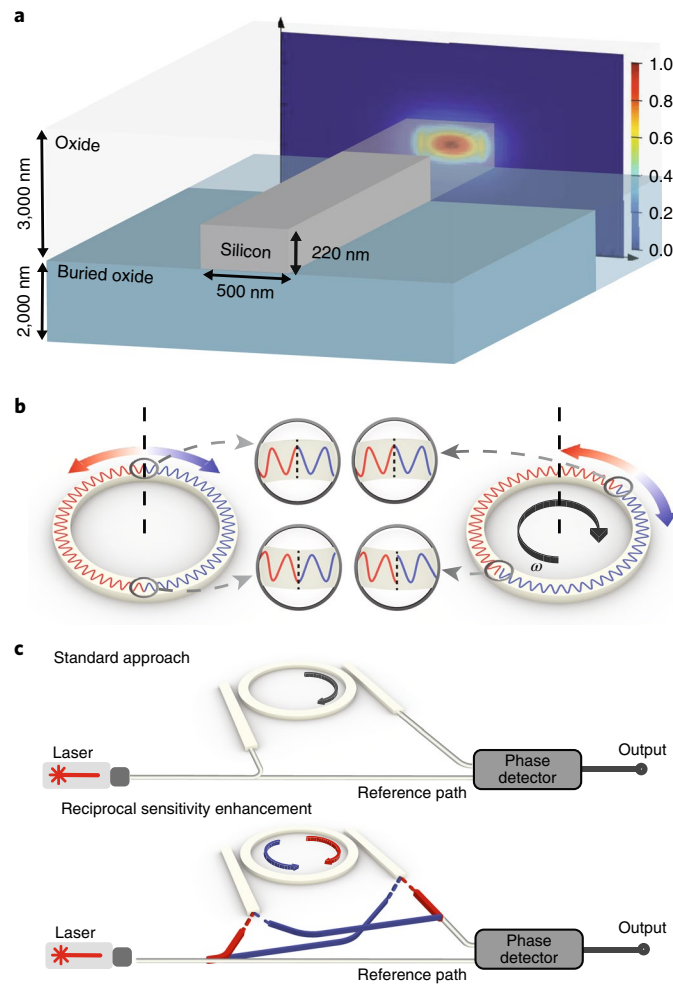


**Fig. 1 | Silicon photonics and the Sagnac effect.** **a**, The silicon nanophotonic waveguide and a mode simulation that shows a single mode at 1,550 nm. **b**, Two light beams travel through the ring, one clockwise and one anticlockwise. While the ring is stationary, the two light beams meet perfectly in phase at the output. However, rotation of the ring induces a phase difference between the two waves, known as the Sagnac phase shift. **c**, Implementation of the reciprocal sensitivity enhancement technique. Unlike the standard approach, the incoming signal is switched between the red path (clockwise propagation) and the blue path (anticlockwise propagation).

enhancement offers an architecture that greatly reduces all sources of noise. This is due to the temporal separation between the clockwise and anticlockwise propagating beams in each path as well as the cancellation of thermal fluctuations using high-frequency optical switching. Critically, this method is more tolerant to the propagation loss of the medium.

The signal can also be amplified without increasing the size of the interferometer by using ring resonators to replace the circular path<sup>25–27</sup>. The phase response of ring resonators amplifies the observed phase difference for a given Sagnac phase shift (Fig. 2a). Thus, to the first order, the phase at the output of the ring resonator,  $\sigma_{\text{Sagnac}}$ , is given by

$$\sigma_{\text{Sagnac}} \approx S \times \Delta\varphi_{\text{Sagnac}} \equiv \frac{Q\lambda}{\pi nL} \Delta\varphi_{\text{Sagnac}} \quad (2)$$

where  $Q$  is the quality factor of the ring resonator and  $L$  is the circumference of the ring. Note that  $S$  can be interpreted as the effective number of times that light travels around the ring before exiting.

Another significant challenge with the standard approach shown in Fig. 1c is the large  $dn/dT$  in silicon that results in

substantial temperature-dependent phase variation between the signal and reference paths. These two path lengths can be made equal by using two identical rings—in lieu of a reference path—which carry light in opposite directions (Fig. 2b). This can significantly alleviate such thermal fluctuations that are substantially different between the ring and the reference path (Fig. 1c). Thus, a system with two rings is only sensitive to spatial gradients in the temperature between the rings. In addition, because the two rings are in close proximity, the resonance peaks will move in a correlated fashion.

We computed the responses of the two rings. Note that, to have a measurable signal, we need to introduce a phase shift  $\varphi_{\text{applied}}$  as an offset phase shift at the output of ring 1. Therefore, the output electric field phasors of ring 1 ( $\vec{E}_1$ ) and ring 2 ( $\vec{E}_2$ ) can be written as

$$\begin{aligned} \vec{E}_1 &= E_1 e^{j(\varphi_1 + \Delta\theta_{\text{thermal}}(t) + \varphi_{\text{applied}} + \sigma_{\text{Sagnac}})} \\ \vec{E}_2 &= E_2 e^{j(\varphi_2 - \sigma_{\text{Sagnac}})} \end{aligned} \quad (3)$$

where  $E_1$  and  $E_2$  are the magnitudes of the output fields,  $\varphi_1$  and  $\varphi_2$  are the phase responses of each ring resonator, and  $\Delta\theta_{\text{thermal}}(t)$  is the

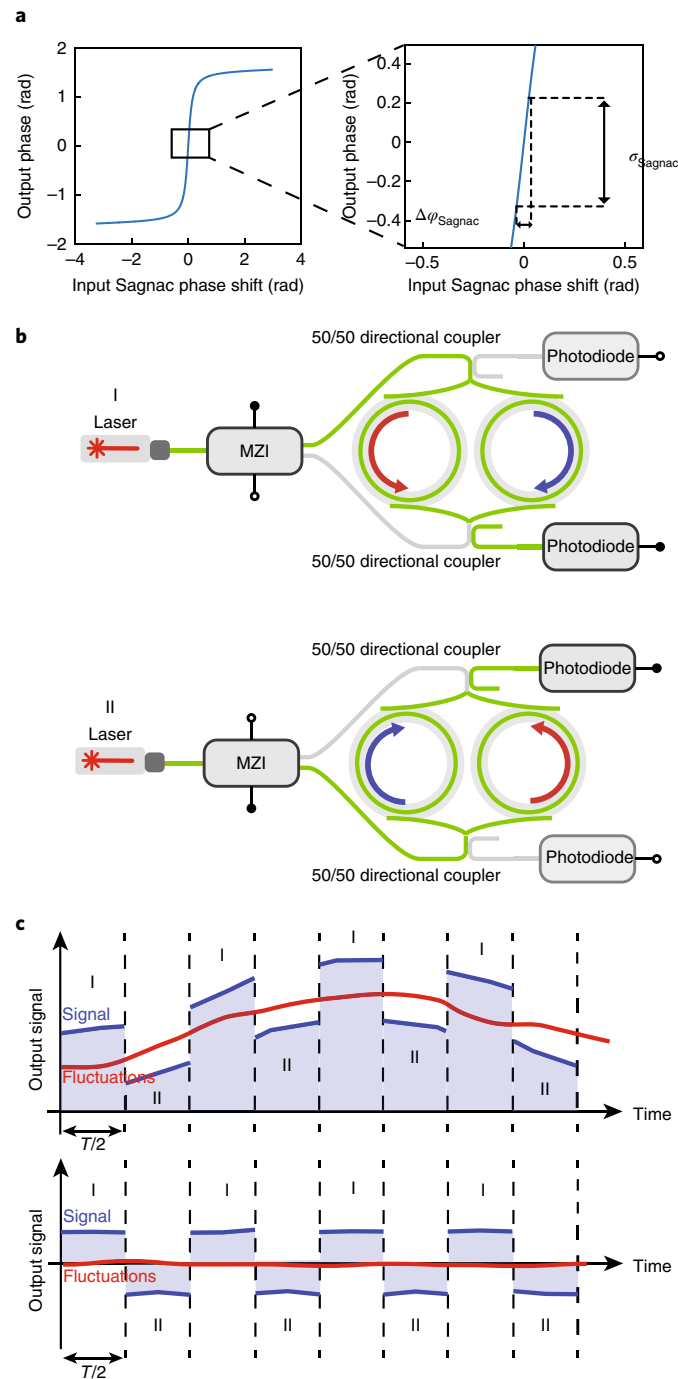


**Fig. 2 | Ring resonator response and system architecture.** **a**, Simulated phase response of the designed microring resonator. **b**, By using a Mach-Zehnder interferometer (MZI), the ring resonators can be fed from two different directions (I and II), and the output toggles between two photodiodes. **c**, By adding the two outputs together, information ‘moves’ to the switching frequency and becomes unaffected by thermal drift.

phase shift difference between two rings due to temperature gradient fluctuations.

Next, the output signal, which we will denote  $Y(t)$ , is proportional to the square magnitude of the sum of these two electric fields:

$$\begin{aligned}
 Y(t) &= |\widetilde{E}_1 + \widetilde{E}_2|^2 \\
 &= E_1^2 + E_2^2 + 2E_1E_2 \cos[\varphi_1 - \varphi_2 + \varphi_{\text{applied}}] \\
 &\quad + \Delta\theta_{\text{thermal}}(t) + 2\sigma_{\text{Sagnac}}
 \end{aligned}
 \tag{4}$$

Now by alternating the direction that rings are fed, we arrive at (Fig. 2b):

$$Y(t) = \begin{cases} +X(t)|\Delta\varphi_{\text{Sagnac}}| + U(t), & 0 < t < \frac{T}{2} \\ -X(t)|\Delta\varphi_{\text{Sagnac}}| + U(t), & \frac{T}{2} < t < T \end{cases}
 \tag{5}$$

where  $T$  is the alternating (that is, switching) period and we defined the signal amplitude,  $X(t)$ , and the undesired signal,  $U(t)$ , as

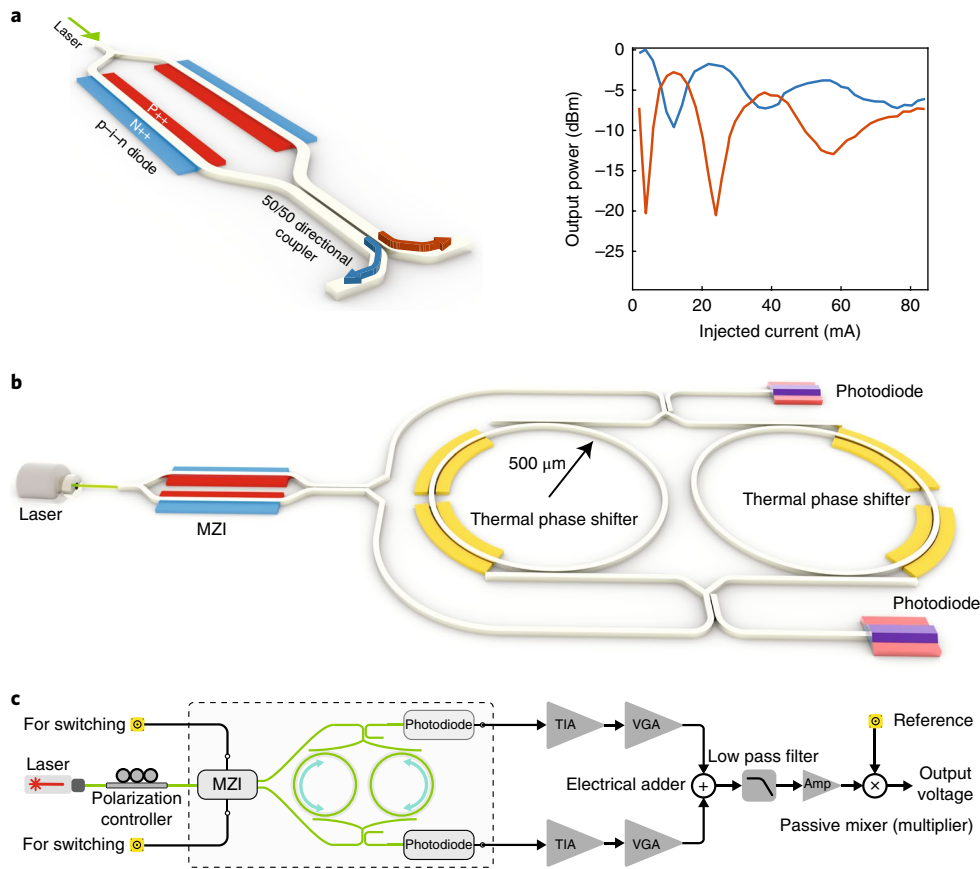


**Fig. 3 | System implementation.** **a**, Design of the input MZI for path switching and the measured power in each direction versus injected current into one of the p-i-n diodes. **b**, Schematic of the implemented NOG. **c**, System architecture with electronic circuitry. Signals from two paths are added together and multiplied by the reference frequency through a passive mixer to extract the amplitude information that encodes the rate of rotation. TIA, transimpedance amplifier; VGA, variable gain amplifier.

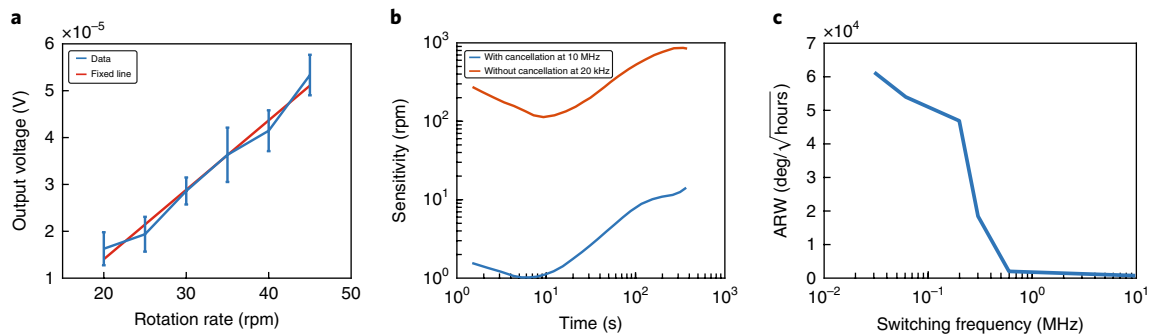


**Fig. 4 | Measurement results.** **a**, Output voltage versus rotation rate. The  $R^2$  value of the linear fit to the data is 0.98. **b**, Measured drift and resultant Allan deviation curves at two different switching frequencies. At 20 kHz, thermal fluctuations and other sources of noise are more pronounced. At 10 MHz, with proper calibration, these effects can be obviated. **c**, ARW measurement for different switching frequencies. This plot shows that lower ARW can be achieved at higher frequencies.

$$\begin{aligned}
 X(t) &= 4SE_1E_2 \sin[\beta(t)] \\
 U(t) &= E_1^2 + E_2^2 + 2E_1E_2 \cos[\beta(t)] \\
 \beta(t) &:= \varphi_1 + \varphi_2 + \varphi_{\text{applied}} + \Delta\theta_{\text{thermal}}(t)
 \end{aligned}
 \tag{6}$$

As is shown in equation (6),  $U(t)$  and  $X(t)$  are, in general, stochastic processes because they depend on thermal fluctuations.

Moreover, if we alternate directions on a faster timescale than the timescale of the fluctuations (for example, 10 MHz), the fluctuations remain mostly correlated. Therefore, these correlated fluctuations are mostly cancelled by adding the two outputs together and subtracting the common-mode signal (Fig. 2c).

Utilizing reciprocal sensitivity enhancement, we designed and implemented a NOG (Fig. 3b). We measured the sensitivity of the gyroscope by measuring the output voltage for different angular

velocities (Fig. 4a). To demonstrate the efficacy of our reciprocal sensitivity enhancement approach, we measured the Allan deviation to calculate the bias instability (BIS) and the angle random walk (ARW) for two separate scenarios (Fig. 4b): one where the switching frequency was set to 20 kHz, where thermal fluctuations have a more prevalent effect on the output, and one at  $1/T=10$  MHz, where thermal fluctuations are negligible. The results are shown in Fig. 4b. For the former setting ( $1/T=20$  kHz), we measured a BIS of 105 r.p.m. and an ARW of  $97,800^\circ/\sqrt{\text{hours}}$ , whereas the latter setting ( $1/T=10$  MHz) resulted in BIS=1 r.p.m. and ARW =  $650^\circ/\sqrt{\text{hours}}$ . The sensitivity at 10 MHz improves by a factor of roughly 100 compared to that at 20 kHz. In addition, measurements of ARW at different switching frequencies show that the threshold frequency for reciprocal sensitivity enhancement is on the order of 100 kHz (Fig. 4c).

In summary, we have introduced reciprocal sensitivity enhancement, which can be used in fibre-optic gyroscopes of all platforms and scales to increase their sensitivity significantly. Our all-integrated optical gyroscope occupies only 2 mm<sup>2</sup> and detects the smallest recorded phase shift (3 nrad) of all miniaturized approaches implemented in silicon nanophotonics so far. We thus show the feasibility of an integrated silicon nanophotonics platform for developing optical gyroscopes.

### Online content

Any methods, additional references, Nature Research reporting summaries, source data, statements of data availability and associated accession codes are available at <https://doi.org/10.1038/s41566-018-0266-5>.

Received: 9 April 2018; Accepted: 4 September 2018;  
Published online: 8 October 2018

### References

- Sagnac, G. Effet tourbillonnaire optique. La circulation de l'éther lumineux dans un interférographe tournant. *J. Phys. Theor. Appl.* **4**, 177–195 (1914).
- Post, E. J. Sagnac effect. *Rev. Mod. Phys.* **39**, 475–493 (1967).
- Gundavarapu, S. et al. Integrated Sagnac optical gyroscope sensor using ultra-low loss high aspect ratio silicon nitride waveguide coil. *Proc. SPIE* **10323**, 103231A (2017).
- Li, J., Suh, M. G. & Vahala, K. Microresonator Brillouin gyroscope. *Optica* **4**, 346–348 (2017).
- Pavesi, L. & Lockwood, D. J. in *Silicon Photonics Vol 94* (eds Pavesi, L., Lockwood, D. J.) 1–50 (Topics in Applied Physics, Springer, Berlin, 2004).
- Asghari, M. & Krishnamoorthy, A. V. Silicon photonics: energy-efficient communication. *Nat. Photon.* **5**, 268–270 (2007).
- Soref, R. The past, present, and future of silicon photonics. *IEEE J. Sel. Top. Quantum Electron.* **12**, 1678–1687 (2006).
- Jalali, B. & Fathpour, S. Silicon photonics. *J. Light. Technol.* **24**, 4600–4615 (2006).
- Lim, A. E. et al. Review of silicon photonics foundry efforts. *IEEE J. Sel. Top. Quantum Electron.* **20**, 405–416 (2014).
- Blanco, A., Chomski, E., Grabtchak, S. & Ibsate, M. Large-scale synthesis of a silicon photonic crystal with a complete three-dimensional bandgap near 1.5 micrometres. *Nature* **405**, 437–440 (2000).
- Culshaw, B. & Kersey, A. Fiber-optic sensing: a historical perspective. *J. Light. Technol.* **26**, 1064–1078 (2008).
- Wei, W., Junlei, X. & Yuxin, X. Research on integrated optical gyroscope. *Proc. ISSCAA* <https://doi.org/10.1109/ISSCAA.2008.4776343> (2008).
- Barrett, B. et al. The Sagnac effect: 20 years of development in matter-wave interferometry. *Comptes Rendus Physique* **15**, 875–883 (2014).
- Lefevre, H. C. *The Fiber-Optic Gyroscope* (Artech House, Norwood, 2014).
- Vaccaro, R. J. & Zaki, A. S. Statistical modeling of rate gyros. *IEEE Trans. Instrum. Meas.* **61**, 673–684 (2012).
- Harris, N. C. et al. Efficient, compact and low loss thermo-optic phase shifter in silicon. *Opt. Express* **22**, 10487–10493 (2014).
- Ciminelli, C., Dell'Olivo, F., Campanella, C. E. & Armenise, M. N. Photonic technologies for angular velocity sensing. *Adv. Opt. Photon.* **2**, 370–404 (2010).
- Buret, T. et al. Fibre optic gyroscopes for space application. *Opt. Fiber Sensors* <https://doi.org/10.1364/OFS.2006.MC4> (2006).
- Davis, J. L. & Ezekiel, S. Closed-loop, low-noise fiber-optic rotation sensor. *Opt. Lett.* **6**, 505–507 (1981).
- Cutler, C. C., Newton, S. A. & Shaw, H. J. Limitation of rotation sensing by scattering. *Opt. Lett.* **5**, 488–490 (1980).
- Ciminelli, C., Peluso, F. & Armenise, M. N. A new integrated optical angular velocity sensor. *Proc. SPIE* **5728**, 93–100 (2005).
- Zhang, Y. et al. A high sensitivity optical gyroscope based on slow light in coupled-resonator-induced transparency. *Phys. Lett. A* **372**, 5848–5852 (2008).
- Vannahme, C. et al. Integrated optical Ti: LiNbO<sub>3</sub> ring resonator for rotation rate sensing. In *Proc. ECIO WE1* (ECIO, 2007).
- Suzuki, K., Takiguchi, K. & Hotate, K. Monolithically integrated resonator microoptic gyro on silica planar lightwave circuit. *J. Light. Technol.* **18**, 66–72 (2000).
- Scheuer, J. & Yariv, A. Sagnac effect in coupled-resonator slow-light waveguide structures. *Phys. Rev. Lett.* **96**, 053901 (2006).
- Ezekiel, S. & Balsamo, S. R. Passive ring resonator laser gyroscope. *Appl. Phys. Lett.* **30**, 478–480 (1977).
- Zhang, H. et al. On-chip modulation for rotating sensing of gyroscope based on ring resonator coupled with Mach–Zehnder interferometer. *Sci. Rep.* **6**, 19024 (2016).

### Acknowledgements

The authors thank A. Khachaturian, B. Hong and B. Abiri for technical discussions.

### Author contributions

P.P.K. and A.H. conceived and designed the device. Simulations and measurements were performed by P.P.K. and A.D.W. Analysis of the results was carried out by P.P.K., A.D.W. and A.H. All authors participated in writing the manuscript.

### Competing interests

The authors declare no competing interests.

### Additional information

**Supplementary information** is available for this paper at <https://doi.org/10.1038/s41566-018-0266-5>.

**Reprints and permissions information** is available at [www.nature.com/reprints](http://www.nature.com/reprints).

**Correspondence and requests for materials** should be addressed to P.P.K.

**Publisher's note:** Springer Nature remains neutral with regard to jurisdictional claims in published maps and institutional affiliations.

© The Author(s), under exclusive licence to Springer Nature Limited 2018

## Methods

To implement this system in silicon photonics, we designed two ring resonators with radius of 500  $\mu\text{m}$  (Supplementary Fig. 2a). These microrings introduced a 30 nrad phase shift at 10 r.p.m. To switch the direction in which the rings were fed, we constructed a Mach-Zehnder interferometer (MZI) consisting of two p-i-n diodes (Fig. 3a) and a 50/50 directional coupler. To read the output from each direction, we built two phase detectors consisting of an optical adder to combine the paths (Y junction) and a photodiode to read the combined power (the germanium photodiode converts input optical light to electrical current; the responsivity is  $0.5 \text{ A W}^{-1}$ ). Each current (one from each direction) was converted to voltage with a transimpedance amplifier (TIA) and amplified with a variable gain amplifier to obtain  $A_1$  and  $A_2$ , the respective gain of each arm in the electronic circuitry (Supplementary Section 'Tuning process'). The signals were then added together and multiplied by a reference frequency through a passive mixer to extract the amplitude information encoding the rotational rate (Fig. 3c).

A low-linewidth distributed feedback (DFB) laser and an off-chip polarization controller were used as the input light at 1,550 nm. This gyroscope was measured and calibrated using a high-accuracy mechanical rotary stage.

**Fabrication.** The silicon nanophotonic chip was fabricated using a silicon-on-insulator process with 2  $\mu\text{m}$  buried oxide, covered by 3  $\mu\text{m}$  oxide.

**Calibrations and measurements.** A calibration process was performed before measuring the rotation rates (see Supplementary Information).

The rotation rate measurements were performed by rotating the whole set-up using a high-precision rotary stage at different rates. At each rotation rate, the output was measured five times and the mean and standard deviation were reported.

## Data availability

The data that support the plots within this paper and other findings of this study are available from the corresponding author upon reasonable request.